ELSEVIER

Journal of Alloys and Compounds 330–332 (2002) 208–214

Journal of ALLOYS AND COMPOUNDS

www.elsevier.com/locate/jallcom

Hydrogen cycling induced degradation in $LaNi_5$-type materials

J.-M. Joubert[a,*], M. Latroche[a], R. Černý[b], A. Percheron-Guégan[a], K. Yvon[b]

[a]*Laboratoire de Chimie Métallurgique des Terres Rares, ISCSA, CNRS, 2–8 rue Henri Dunant, 94320 Thiais Cedex, France*
[b]*Laboratoire de Cristallographie, Université de Genève, 24 Quai Ernest Ansermet, 1211 Genève 4, Switzerland*

Abstract

Defect generation in hydrogen cycled $LaNi_5$ and substituted derivatives was studied in previous work by analysis of the X-ray line broadening. In the present work, the pulverization in the same samples is analyzed by granulometric measurements and scanning electron microscopy. Both phenomena correspond to irreversible degradation of the initial intermetallic compounds, as confirmed by first cycle hysteresis presence in pressure composition isotherms. They are analyzed in terms of the lattice expansion occurring at the discrete phase transition between α and β phases and measured by X-ray diffraction. This study shows that, in addition to this latter parameter, the limit of elasticity and the resistance to rupture must be considered.

Keywords: Hydrogen storage materials; Intermetallics; Gas-solid reactions; Dislocations and disclinations; X-ray diffraction

1. Introduction

Hydrogen absorption and desorption cycling has two main physical and irreversible consequences on $LaNi_5$-type intermetallic compounds: defect generation and pulverization. Both phenomena can have a dramatic influence on the properties of those compounds regarding the applications. While defect generation leads to amorphisation and capacity decrease after prolonged cycling [1], decrepitation results in increasing the surface exposed to passivation or corrosion either in solid-gas or electrochemical applications. Both phenomena are thought to originate from the lattice expansion occurring at the phase transition between the intermetallic and the hydrided compound. Following the work of Wu et al. [2], careful investigation of the hydrogen induced X-ray line broadening was undertaken in previous work with the use of synchrotron radiation for $LaNi_5$ and 16 different substitutional derivatives [3]. The strains observed were interpreted in terms of dislocation formation whose natures and densities were refined. In the present work, our aim is to carefully investigate the relationships between the hydrogenation induced lattice expansion, the hysteresis of the pressure–composition isotherm and the degradation in terms of dislocation generation or decrepitation.

2. Previous work

The defects generated by hydrogen absorption–desorption cycling were studied by analysis of the line broadening observed in synchrotron X-ray powder diffraction patterns [3] following a method similar to the one used by Wu et al. [2]. The data were fitted by using two different dislocation systems E1 ($1/3\langle -2110\rangle(0001)$) and E2 ($1/3\langle -2110\rangle(0{-}110)$), both with Burgers vector **a** but gliding in the basal or prismatic planes, respectively. Both dislocation systems originate from misfit dislocations accommodating the difference of the *a* lattice parameters of the α and of the β phases. As a function of the substitution, two main effects were observed: decrease of the broadening associated with a reduction of the total dislocation density and modifications of the anisotropy of the line broadening associated with changes of the dislocation system involved. It was shown that $LaNi_5$ and $LaNi_{4.25}Co_{0.75}$ samples contain essentially E2 dislocations in high quantities while dislocations of the E1 type are dominant in manganese substituted compounds. The changes of the dislocation system was attributed to changes of the hydride precipitate shape coherently growing in the intermetallic matrix: a high E1 content would correspond to a precipi-

*Corresponding author.
E-mail address: jean-marc.joubert@glvt-cnrs.fr (J.-M. Joubert).

0925-8388/02/$ – see front matter
PII: S0925-8388(01)01640-1

tate growth in the basal plane while a high E2 content would correspond to a needle- or platelet-like growth of the hydride precipitate parallel to the *c*-axis. In contrast with those samples where the dislocation density is high, aluminium substituted compounds (including the bisubstituted and trisubstituted $LaNi_{3.95}Al_{0.3}Co_{0.75}$ and $LaNi_{3.55}Mn_{0.4}Al_{0.3}Co_{0.75}$) show dislocation content reduced to a very low density.

3. Experimental

As described in Ref. [3], the intermetallic compounds were synthesised by induction melting of the pure elements followed by a suitable annealing. Their single phase character and compositional homogeneity were checked by X-ray diffraction (XRD), optical metallography and electron probe micro-analysis. The pressure composition isotherm (PCI) curves were measured with a conventional Sievert's type apparatus. In order to measure the discrete lattice parameter expansion occurring during the formation of the hydride phase (β), X-ray diffractograms have been obtained in air at room temperature on samples partially hydrogenated, after 5 cycles, up to an intermediate concentration on the pressure plateau at 25°C and, thus, showing equilibrium between saturated solid solution in the intermetallic compound (α_{max}) and undersaturated β_{min} phases. Less stable hydride samples were mixed with vacuum grease before the measurement to prevent desorption during the time of the experiment. The X-ray diffractograms were analyzed by the Rietveld method. So-called cycled compounds, used also for the line broadening experiments [3], were obtained, as detailed in that work, by hydrogen absorption and desorption cycling for 15 cycles at 40°C. Mean particle size (*G*) of those sample has been measured by a laser granulometer. Scanning electron microscopy (S.E.M.) was also performed on the cycled samples to investigate the grain morphology.

4. Results

The lattice parameters of α_{max} and β_{min} phases, measured by XRD, are reported in Table 1, except for $La_{0.5}Ce_{0.5}Ni_5$ sample which exhibits a plateau pressure too high to be measured. The relative discrete lattice parameter expansion $\Delta a/a$, $\Delta c/c$ and the volume expansion $\Delta V/V$ are derived from this measurement. The comparison of our results with the literature data on $LaNi_5$, $LaNi_4Cu$ and $LaNi_{3.55}Mn_{0.4}Al_{0.3}Co_{0.75}$ for which measurements by in situ techniques have already been reported [4,5], validates our ex situ measurement procedure. The PCI curves at 40°C have been measured for several samples during the first absorption cycle and for all the samples during the 6th cycle. They are shown for selected samples in Fig. 1. Those measurements allow the derivation of the hysteresis factor ($H = 1/2.RT \ln (P_{abs}/P_{des})$) as defined by Quian et al. [6] which are reported in Table 2.

The plateau lengths observed on the PCI curves are in agreement with discrete volume expansions measured by XRD. This means that the volume expansion depends only on the hydrogen concentration whatever the nature of the sample. Clear plateau shortening is observed for all the cobalt substituted samples. In $LaNi_{4.25}Co_{0.75}$ and $LaNi_3Co_2$, the presence of a second hydride phase, as evidenced in $LaNi_2Co_3$ [7], was not evident in either PCI or XRD measurements. Contrary to what is indicated in Ref. [7], the β phase of $LaNi_3Co_2$ shows the same strong orthorhombic distortion as evidenced for $LaNi_2Co_3H_{3.2}$.

All the substituting elements tend to decrease the large

Table 1
Lattice parameters of the intermetallic compounds, saturated α and undersaturated β phases, and relative discrete lattice expansions

Compound	Intermetallic compound			Saturated α phase			Under-saturated β phase			Relative discrete lattice expansion		
	a (Å)	c (Å)	V (Å^3)	a (Å)	c (Å)	V (Å^3)	a (Å)	c (Å)	V (Å^3)	$\Delta a/a$ (%)	$\Delta c/c$ (%)	$\Delta V/V$ (%)
$LaNi_5$	5.018	3.982	86.82	5.025	3.996	87.38	5.393	4.248	107.00	7.3	6.3	22.4
$LaNi_{4.6}Mn_{0.4}$	5.045	4.015	88.51	5.051	4.019	88.80	5.387	4.246	106.71	6.7	5.6	20.2
$LaNi_4Mn$	5.092	4.068	91.36	5.102	4.077	91.91	5.380	4.278	107.23	5.4	4.9	16.7
$LaNi_{4.9}Al_{0.1}$	5.023	3.988	87.15	5.033	3.993	87.60	5.382	4.217	105.78	6.9	5.6	20.8
$LaNi_{4.7}Al_{0.3}$	5.034	4.008	87.96	5.044	4.008	88.31	5.352	4.147	102.87	6.1	3.5	16.5
$LaNi_{4.25}Co_{0.75}$	5.029	3.984	87.24	5.037	3.991	87.69	5.304	4.043	98.50	5.3	1.3	12.3
$LaNi_3Co_2$	5.045	3.986	87.85	5.060	3.993	88.54	*	4.115	98.30	*	3.1	11.0
$LaNi_{4.3}Mn_{0.4}Al_{0.3}$	5.061	4.042	89.66	5.065	4.040	89.76	5.346	4.200	103.95	5.5	4.0	15.8
$LaNi_{3.85}Mn_{0.4}Co_{0.75}$	5.050	4.016	88.72	5.064	4.024	89.37	5.322	4.123	101.13	5.1	2.5	13.2
$LaNi_{3.95}Al_{0.3}Co_{0.75}$	5.042	4.013	88.34	5.067	4.017	89.32	5.293	4.094	99.33	4.5	1.9	11.2
$LaNi_{3.94}Mn_{0.4}Al_{0.3}Co_{0.36}$	5.066	4.045	89.93	5.085	4.052	90.74	5.315	4.163	101.85	4.5	2.7	12.2
$LaNi_{3.55}Mn_{0.4}Al_{0.3}Co_{0.75}$	5.069	4.044	89.97	5.100	4.058	91.41	5.291	4.145	100.49	3.7	2.1	9.9
$LaNi_4Fe$	5.050	4.022	88.84	5.064	4.023	89.35	5.320	4.117	100.91	5.1	2.3	12.9
$LaNi_4Cu$	5.039	4.007	88.10	5.057	4.024	89.12	5.378	4.150	103.95	6.3	3.1	16.6

* The β phase of $LaNi_3Co_2$ is orthorhombic with lattice parameters $a = 8.982$ Å, $b = 5.318$ Å, $c = 4.115$ Å. As this cell is derived from the $CaCu_5$ cell following $a_{orth} = a_{hex}.\sqrt{3}$, $b_{orth} = a_{hex}$, $c_{orth} = c_{hex}$, the volume expansion related to the hexagonal cell has been easily calculated and is given in Table 1.

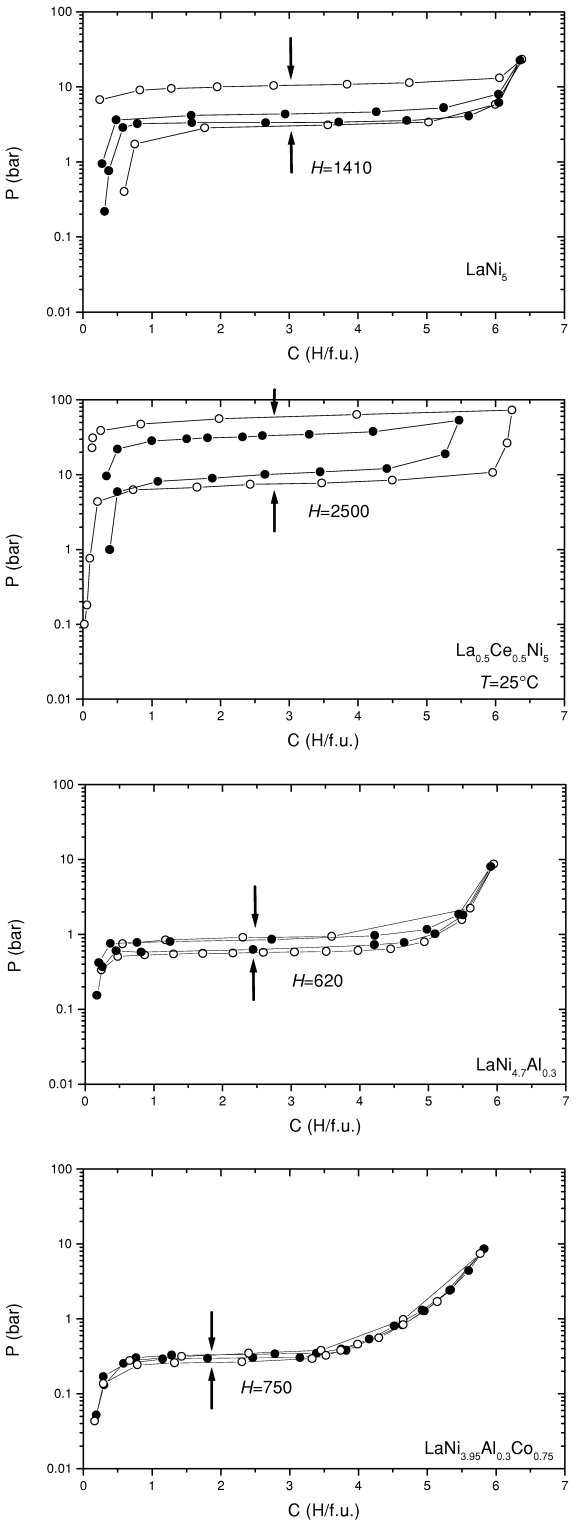

Fig. 1. PCI curves at 40°C (except for $La_{0.5}Ce_{0.5}Ni_5$: 25°C) at the 1st (open symbols) and 6th (full symbols) hydrogenation cycles for selected samples.

and nearly isotropic lattice expansion occurring at the phase transition between $LaNi_5$ and its hydride. Among them cobalt has a peculiar role because the decrease is large and because the $\Delta c/c$ value is decreased far more than the $\Delta a/a$ value. Additional effects are observed by combining the substituents in multi-substituted compounds and the trisubstituted $LaNi_{3.55}Mn_{0.4}Al_{0.3}Co_{0.75}$ has the smallest volume expansion of all the compounds studied.

The granulometric measurements were performed on all samples. A gaussian distribution of the particle size was generally observed and G values are given in Table 2. The majority of the cycled samples were examined by S.E.M. and the observations confirmed the mean sizes given. The mean grain size measured on $LaNi_5$ (22 μm) and $LaNi_{4.9}Al_{0.1}$ (12 μm) samples are in contradiction with those found by Belkbir et al. on the same compositions by S.E.M. observation after eleven cycles (5 and 10 μm respectively) [8]. However, our measurement was repeated on other samples and confirmed our first finding. The substitution of $LaNi_5$ by elements like Mn, Al or Cu, even at a very low level (e.g. $LaNi_{4.9}Al_{0.1}$) drastically reduces the grain size after cycling.

5. Discussion

As it is generally accepted that the dislocations generated during hydrogen cycling originate from the misfit of the lattice parameters between α and β phases, one would expect that the measurement of the discrete lattice expansion would give insight into the different behaviours observed toward hydrogen induced dislocation generation. However, plots of E2 and E1 (both with Burgers vector **a**) dislocation densities against the lattice parameter expansions do not show any evident correlation. $LaNi_5$ presents the largest $\Delta a/a$ value (+7.3%) and shows one of the highest E2 dislocation density. Consistently, $LaNi_{3.55}Mn_{0.4}Al_{0.3}Co_{0.75}$ shows the smallest $\Delta a/a$ (+3.7%) and one of the lowest dislocation density among the samples studied. But, the two cases of $LaNi_{4.7}Al_{0.3}$ which shows high $\Delta a/a$ value (+6.1%) but low dislocation density and of $LaNi_4Mn$ showing smaller $\Delta a/a$ value (+5.4%) and one of the highest total dislocation density contradict the hypothesis of a direct correlation between these two parameters. Neither can the total lattice expansion occurring at each cycle, between fully desorbed and saturated samples, be the key factor because as we have shown, it is directly related to the total capacity which does not vary in the same way as the dislocation density. Samples with the same $\Delta V/V$ i.e. subjected to the same strain during hydrogenation, do not exhibit the same dislocation density, i.e. the same plastic deformation. This proves that the elastic limit has to be taken into account and that it must be different depending on the samples.

In Fig. 2, the measured mean particle size is plotted as a function of the relative discrete volume expansion ($\Delta V/V$). It can be globally observed that G decreases for high $\Delta V/V$ values. However, exceptions can be found, for e.g. $LaNi_5$ which presents the highest $\Delta V/V$ value but still has a high G value of around 20 μm (confirmed by S.E.M. observa-

Table 2
Absorption (P_{abs}) and desorption (P_{des}) plateau pressures and hysteresis factor ($H = 1/2.RT\ \ln(P_{abs}/P_{des})$) at the 1st and 6th hydrogenation cycles at 40°C (except *: data at 25°C) mean particle size (G) and total dislocation density (ρ) and fractions E1 and E2 corresponding to the two dislocation systems involved (from Ref. [3])

Compound	1st cycle			6th cycle			G (μm)	ρ (10^{11} cm^{-2})	E1 (%)	E2 (%)
	P_{abs} (bar)	P_{des} (bar)	H	P_{abs} (bar)	P_{des} (bar)	H				
$LaNi_5$	10.50	3.56	1410	4.40	3.35	350	22	2.5	11	89
$LaNi_{4.6}Mn_{0.4}$	0.83	0.33	1200	0.58	0.31	820	10	2.7	36	64
$LaNi_4Mn$	0.0625	0.0078	2710	0.014	0.009	570	11	3.8	64	36
$LaNi_{4.9}Al_{0.1}$				3.05	2.23	410	12	1.2	10	90
$LaNi_{4.7}Al_{0.3}$	0.92	0.57	620	0.86	0.63	400	11	0.29	90	10
$LaNi_{4.25}Co_{0.75}$	4.33	1.5	1380	1.90	1.65	180	34	2.0	2	98
$LaNi_3Co_2$				0.64	0.50	320	40	0.34	11	89
$LaNi_{4.3}Mn_{0.4}Al_{0.3}$	0.123	0.070	730	0.096	0.079	250	8	1.1	88	12
$LaNi_{3.85}Mn_{0.4}Co_{0.75}$	0.39	0.25	580	0.33	0.24	410	13	0.62	87	13
$LaNi_{3.95}Al_{0.3}Co_{0.75}$	0.33	0.26	310	0.33	0.30	120	20	0.045	89	11
$LaNi_{3.94}Mn_{0.4}Al_{0.3}Co_{0.36}$	0.074	0.047	590	0.056	0.047	230	14	1.7	79	21
$LaNi_{3.55}Mn_{0.4}Al_{0.3}Co_{0.75}$	0.050	0.031	750	0.040	0.038	70	21	0.17	92	8
$LaNi_4Fe$	1.60	0.92	720	1.15	0.97	220	18	0.84	14	86
$LaNi_4Cu$	4.10	1.53	1280	2.50	1.83	400	9	0.35	69	31
$La_{0.5}Ce_{0.5}Ni_5$	58*	7.7*	2500*	32.0*	10.0*	1440*	16	4.9	46	54

tions). Similarly, Co substituted samples also present larger particle sizes than expected from their volume expansion. This shows that, once again, the lattice expansion is not the only factor responsible for decrepitation. The different behaviours of $LaNi_5$ and Co substituted compounds must be attributed to higher resistance to rupture of those compounds.

Some examples of PCI curves measured at the first hydrogen cycle and after hydrogen activation are shown in Fig. 1. Plots of the hysteresis factor obtained at the first cycle as a function of the total dislocation density (ρ) is shown in Fig. 3. Fairly good correlation between those two parameters can be observed. The hysteresis in metal–hydrogen systems has been attributed by many authors to the formation of defects related to plastic deformation [9,10]. This has been demonstrated for $LaNi_5$ by Kisi et al. [11], though in that work planar defects were invoked instead of dislocations which were later demonstrated to be the dominant lattice defects [2]. In the present work, we confirm this assumption by extending this analysis to samples which exhibits higher and lower hysteresis factors and by showing that it corresponds to higher and lower dislocation densities, respectively. In addition to this result, one can notice that, on most samples, only the absorption

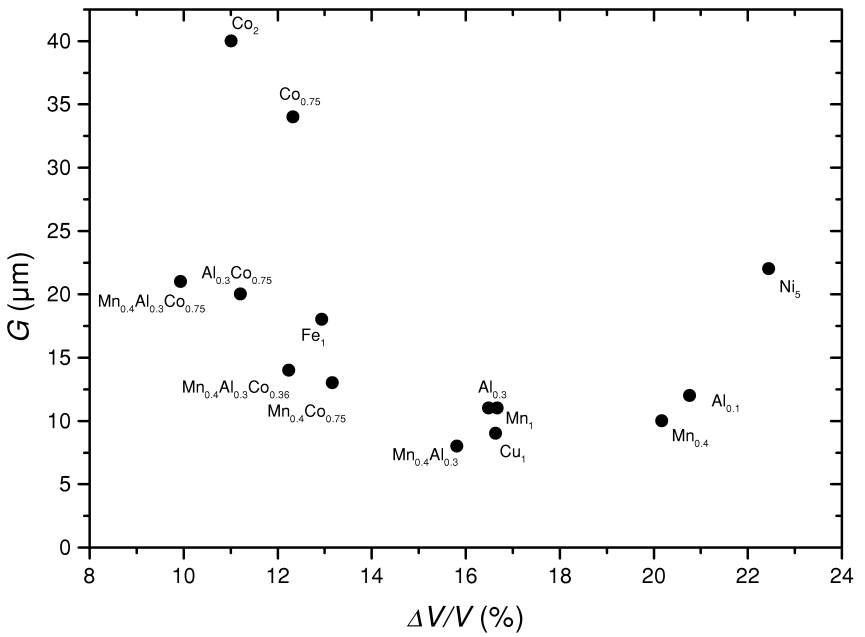

Fig. 2. Mean particle size (G) of hydrogen cycled samples $LaNi_{5-x}M_x$ as a function of the relative discrete lattice expansion ($\Delta V/V$).

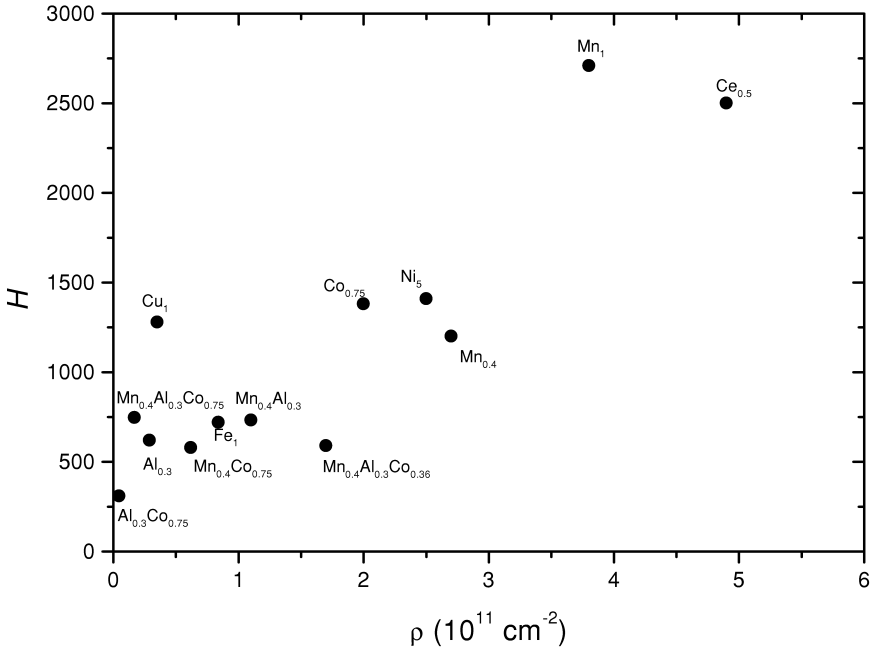

Fig. 3. Hysteresis factor ($H = 1/2.RT\ \ln(P_{abs}/P_{des})$) at the 1st hydrogenation cycle of $LaNi_{5-x}M_x$ and $La_{0.5}Ce_{0.5}Ni_5$ compounds as a function of the total dislocation density (ρ) in hydrogen cycled samples.

curve is significantly modified at the first cycle indicating that the defect generation occurs essentially during the first absorption as stated in Refs. [11,12]. The good correlation obtained between H and ρ shows that a large hysteresis is the consequence of the energy loss due to irreversible dislocation formation more than that due to the decrepitation.

Two examples of the grain morphology after hydrogen cycling are presented in Fig. 4. Strong differences can be observed. $LaNi_{4.25}Co_{0.75}$ shows after hydrogen cycling a rather peculiar morphology with very torn surfaces together with cleaved faces on the same grain. It has been possible to pick up single crystals of a size ~50 μm in the powdered sample. The direction of the fiber-like shapes occurring at the grain surface was unambiguously identified after single crystal XRD analysis as being of the [00*l*] type. Some of the cleaved surfaces, but not every, were identified as being of the 00*l* type. All the samples studied were really single crystals, though strong misorientations of mosaic blocks could be observed around the *c** axis. In fracture studies, such torn surfaces are interpreted as the consequence of a ductile fracture occurring

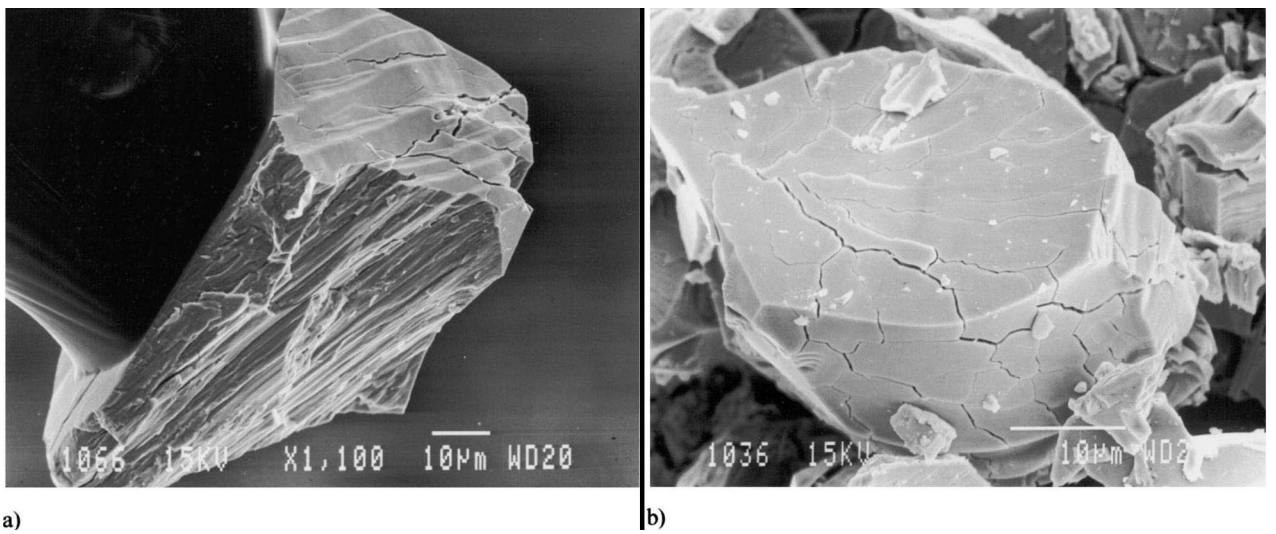

Fig. 4. S.E.M. observation of $LaNi_{4.25}Co_{0.75}$ (a) and of $LaNi_{3.55}Mn_{0.4}Al_{0.3}Co_{0.75}$ (b) after hydrogen cycling. $LaNi_{4.25}Co_{0.75}$ sample is a single crystal glued on the top of a glass needle. The direction of the fibers is [00*l*], and the indexation of the plane is 00*l*, as obtained after orientation of the crystal with a single crystal diffractometer.

after severe plastic deformation, while cleaved surfaces are generated after brittle fracture i.e. occurring with little plastic deformation. This observation is in perfect agreement with our finding that E2 dislocations with Burgers vector **a** and gliding in the prismatic planes are exclusively present in this sample. Those dislocations contribute to the ductile fracture of the grains. The absence of any dislocation gliding in the basal plane leads to a brittle fracture along this plane, giving rise to cleaved surfaces. In addition to that, the fiber-like shapes observed at the surface give a strong support to the idea formulated in [3] of growth of the hydride precipitate in the [00*l*] direction. It explains also the strong needle-like [00*l*] preferential orientation observed after Rietveld refinement of XRD patterns of cycled compounds (see for example Fig. 2 of Ref. [3]).

On the contrary, the trisubstituted $LaNi_{3.55}Mn_{0.4}Al_{0.3}Co_{0.75}$ shows only cleaved surfaces in agreement with the absence of any type of dislocations in this sample. These examples demonstrate that the microstructure of the decrepitated grain can be interpreted in terms of the defects observed on the nanometer scale.

Considering the possible links between decrepitation and dislocation generation, Fig. 5 shows that, once again, no simple relationship exists. While $LaNi_{4.25}Co_{0.75}$ shows high dislocation content and high resistance to decrepitation, manganese substituted compounds with dislocation density of the same order of magnitude pulverize easily. The same order of magnitude of the granulometry is obtained for $LaNi_{4.7}Al_{0.3}$ which is resistant to dislocation induction. Finally, $LaNi_{3.95}Al_{0.3}Co_{0.75}$ or $LaNi_{3.55}Mn_{0.4}Al_{0.3}Co_{0.75}$ shows both high resistance to dislocation generation and low decrepitation. These two latter compounds take advantage of the synergetic substitution by Al and Co. While Al clearly reinforces the resistance to dislocation generation, Co increases strongly the resistance to the pulverization.

The influence of the resistance to defect generation on the electrochemical properties has not yet been demonstrated. However, the exceptional resistance to dislocation generation together with reduced decrepitation in the trisubstituted $LaNi_{3.55}Mn_{0.4}Al_{0.3}Co_{0.75}$ could be an explanation of the exceptional behaviour of the trisubstitution as far as electrode cycle life is concerned [13]. If this assumption is true, one could predict similar cycling properties for the bisubstituted $LaNi_{3.95}Al_{0.3}Co_{0.75}$. This compound has a larger capacity in solid-gas reaction due to the absence of manganese (5.7 H/f.u. against 5.4 H/f.u. under 10 bar pressure). Considering that, for industrial materials, the differences in terms of plateau pressure for manganese deficient compounds could be compensated by lanthanum enrichment of the mischmetal, reduction of the manganese concentration could be suggested as an interesting route to increase the capacity without any deterioration of the cycle life.

6. Conclusion

Dislocation generation and pulverization in $LaNi_5$ and substituted derivatives are both irreversible effects and originate from the lattice expansion induced by the hydride formation. The consequence of the irreversibility is an increased hysteresis at the first hydrogenation cycle, mainly originating from the defect generation. Consequences of the defect generation and of the hydride growth process on

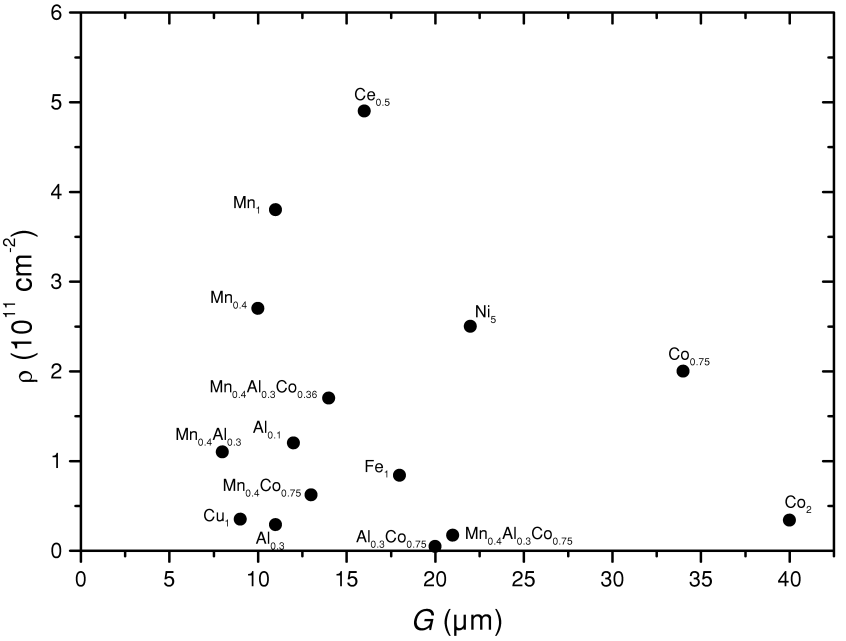

Fig. 5. Total dislocation density (ρ) in hydrogen cycled $LaNi_{5-x}M_x$ and $La_{0.5}Ce_{0.5}Ni_5$ compounds as a function of the mean particle size (G).

the grain morphology can be found in some samples (e.g. $LaNi_{4.25}Co_{0.75}$). However, dislocation densities observed in the cycled samples do not correlate with the mean particle sizes because the elastic limit in one case and the resistance to rupture in the other case must be considered together with the strain caused by the discrete lattice expansion. Those parameters, difficult to measure for such samples, are shown to depend strongly on the substituted element and the substitution rate. Whatever the application, gas or electrochemical storage, we believe that both the pulverization and the resistance to defect generation need to be reduced. The combination of aluminium and cobalt substitution has been demonstrated to have positive effects on those two parameters.

Acknowledgements

The authors wish to thank L. Touron and E. Leroy for the microprobe analyses, F. Briaucourt for technical assistance and A. Rivière for help with the use of the S.E.M.

References

[1] S.W. Lambert, D. Chandra, W.N. Cathey, F.E. Lynch, R.C. Bowman Jr., J. Alloys Comp. 187 (1992) 113–135.
[2] E. Wu, E.H. Kisi, E. Mac. A. Gray, J. Appl. Crystallogr. 31 (1998) 363–368.
[3] R. Černý, J.-M. Joubert, M. Latroche, A. Percheron-Guégan, K. Yvon, J. Appl. Crystallogr. 33 (2000) 997–1005.
[4] P.H.L. Notten, J.L.C. Daams, R.E.F. Einerhand, J. Alloys Comp. 210 (1994) 233–241.
[5] M. Latroche, A. Percheron-Guégan, F. Bourée-Vigneron, J. Alloys Comp. 265 (1998) 209–214.
[6] S. Quian, D.O. Northwood, Z. Phys. Chem. 164 (1989) 1349.
[7] H.H. Van Mal, K.H.J. Buschow, F.A. Kuijpers, J. Less-Common Met. 32 (1973) 289–296.
[8] L. Belkbir, E. Joly, N. Gerard, J.-C. Achard, A. Percheron-Guégan, J. Less-Common Met. 73 (1980) 69–77.
[9] R. Balasubramaniam, J. Alloys Comp. 253–254 (1997) 203–206.
[10] T.B. Flanagan, J.D. Clewley, J. Less-Common Met. 83 (1982) 127–141.
[11] E.H. Kisi, C.E. Buckley, E.M. Gray, J. Alloys Comp. 185 (1992) 369–384.
[12] M.P. Pitt, E. Mac. A. Gray, E.H. Kisi, B.A. Hunter, J. Alloys Comp. 293–295 (1999) 118–123.
[13] H. Ogawa, M. Ikoma, H. Kawano, I. Matsumoto, J. Power Sources 12 (1988) 393–410.